Computational Characterization of Low-Lying States and Intramolecular Charge Transfers in *N*-Phenylpyrrole and the Planar-Rigidized Fluorazene

Xuefei Xu, Zexing Cao,* and Qianer Zhang

Department of Chemistry, State Key Laboratory of Physical Chemistry of Solid Surfaces, Xiamen University, Xiamen 361005, China

Received: October 6, 2005; In Final Form: November 20, 2005

Low-lying states and intramolecular charge transfers in *N*-phenylpyrrole (PP) and its planar-rigidized derivative fluorazene (FPP) have been investigated by ab initio methodologies. On the basis of calculations, properties of the excited states and plausible dual-fluorescence mechanisms have been elucidated. Present results show that S_2 as a key state is involved in the consecutive photophysical processes. The S_2 state is easily populated under excitation. In the polar MeCN solution, S_2 can evolve to either a lower-energy locally excited state or a lower-energy solvated intramolecular charge-transfer state (S-ICT). The former emits a normal fluorescence back to the ground state, and the latter is exclusively responsible for the red-shifted fluorescence band. Calculations reveal that the emissive ICT states in both FPP and PP have similar geometric features, an elongated *N*-phenyl bond, a pyramidal carbon atom linking the pyrrole ring, and a quinonoid phenyl ring. The twisting of molecule around the *N*-phenyl bond is not necessary for the intramolecular charge transfer. Predicted absorption and emission spectra are in reasonable agreement with the experimental observations.

Introduction

Since 4-dimethylaminobenzonitrile (DMABN) was first discovered to exhibit dual fluorescence in around 1960,[1,2] a large number of electron donor (D)−acceptor (A) molecules have been detected to fluoresce in two different bands when existed in a polar solvent.[3] Along with a normal emission band from the locally excited (LE) state, an unexpected red-shifted emission band appears in polar solvents. The intensity of the so-called anomalous fluorescence depends on the polarity of solvent.

For several decades mechanistic aspects of the dual fluorescence have been discussed extensively. A photoinduced intramolecular charge transfer (ICT) state has been considered to be responsible for the red-shifted band in the dual fluorescence. However, the formation mechanism of the emitting ICT state and its structural features are still controversial up to now. Several structural hypotheses about the emitting ICT state have been proposed: a donor−acceptor perpendicular configuration (the twisted ICT, TICT),[4,5] a planar conformation (the planar ICT, PICT),[6−9] and the structural changes due to rehybridization of donor[10,11] or acceptor.[12,13] On the basis of properties of benzene in the excited state,[14] a planar quinoid geometry (corresponding to PICT) and a twisted anti-quinoid structure (corresponding to TICT) have been employed to elucidate the ICT state. The concepts of the TICT and PICT states among such models have been frequently used to rationalize the dual fluorescence.

In general, the ICT state is formed through two plausible pathways: the adiabatic reaction pathway from LE state to the ICT state[2,15,16] and the nonadiabatic reaction path from the Franck−Condon (FC) structure on S_2 to either ICT or LE via a conical intersection (CI).[17] Recent time-dependent density functional and CASSCF calculations[18,19] show the existence of state-crossing models for the formation of the ICT state. Gómez et al.[20] suggested a mechanistic overview for the dual fluorescence in DMABN, in which an ultrafast nonradiative $S_2 \rightarrow S_1$ decay leads to either S_1-LE or S_1-TICT geometries, and the equilibrium between S_1-LE and S_1-TICT in the adiabatic reaction path controls the dual fluorescence.

Since the most stable structure of the ICT state depends on the specific system and the surroundings, further investigations on the rigidized dual-fluorescence species are highly required.

N-Phenylpyrrole (PP) is a typically flexible D−A molecule, and it has been widely studied both experimentally and theoretically due to its significant photophysical properties.[14,21−34] The emitting ICT state of PP was attributed to a TICT state in previous theoretical calculations.[14,26,27] In the polar solvents, the TICT state with large dipole moment is stabilized to become another minimum on the potential energy surface of the first excited state (S_1) and the barrier from LE to TICT is lowered so that the adiabatic LE↔TICT reaction can take place, sequentially resulting in the red-shifted fluorescence. Nevertheless, the electronic spectra of jet-cooled PP argue the TICT model responsible for the emitting ICT state because there is a relatively larger barrier of 1526 cm^{-1} to perpendicularity compared to that of 105 cm^{-1} to planarity for PP in the S_1 state by its calculated torsional potential.[25]

Recent fluorescence observations reveal that a planar-rigidized fluorazene (FPP) has the ICT behavior similar to that of its flexible counterpart PP, which suggests that the TICT state is also not necessary for the dual fluorescence of PP.[34,35] Because of lack of knowledge in electronic and geometric aspects of the low-lying states in FPP, the nature of the photophysical similarity of FPP and PP is still unclear. FPP and PP have similar π-electron systems and conjugated moieties, which can be used for the case study of the ICT features and the dual-fluorescence mechanism theoretically.

In the present work, extensive theoretical calculations by the density functional theory, complete active space self-consistent field (CASSCF), multiconfigurational second-order perturbation

* To whom correspondence should be addressed. E-mail: zxcao@xmu.edu.cn.

10.1021/jp055695a CCC: $33.50
Published on Web 01/19/2006

theory (CASPT2), and multireference configuration interaction (MRCI) approaches have been performed. Structures and properties of FPP and PP in their low-lying states have been explored. On the basis of calculations, the features of the ICT states and the mechanistic aspects of the dual fluorescence for both species have been discussed.

Computational Details

The CASSCF[36] methodology implemented in the program packages MOLPRO 2002[37] and GAUSSIAN 98[38] has been applied to study of low-lying singlet states in PP and FPP molecules. The CASSCF approach has been recognized to be feasible in determining geometries and dipole moments of low-lying states in comparison with the experimental data, even for the ICT state.[39] In the CASSCF optimization of geometry, 12 valence electrons are allowed to distribute into the active space composed of 11 π orbitals. No symmetry constraints have been introduced in all optimizations of the interested electronic states for the flexible PP molecule in order to locate the lowest-energy structures. For comparison with previous calculations,[14,27] the states with coplanar and perpendicular conformations also have been optimized within C_{2v}-symmetry restriction. Since FPP has the planar rigidized structure, the Cs symmetry has been applied in optimization. In consideration of the effect of ICT on structure, the ICT state was reoptimized fully without symmetry constraints. After the stationary points on the potential-energy surfaces (PES) of the low-lying states were obtained, single-point calculations have been carried out by both MRCI[40] and CASPT2[41] methods incorporating the dynamic correlation effects.

The absorption spectra of PP and FPP were respectively computed by MRCI and CASPT2 approaches in combination of the state-averaged CASSCF calculations at the optimized ground-state geometries. For comparison, the time-dependent density functional approach with the Becke's three-parameter hybrid exchange functional and Lee−Yang−Parr correlation functional[42] (TD-B3LYP) and the CCSD-EOM[43] calculations also have been preformed in determining the vertical transition energies.

Oscillator strengths for electronic transitions were determined as

$$f = \frac{2}{3}\Delta E|D|^2 \quad (1)$$

where $\Delta E = E_a - E_b$ refers to the electronic energy difference in atomic units between the two states and D in eq 1 is the transition moment in atomic units.[44] The corresponding lifetime τ (in seconds) is given by eq 2

$$\tau = \frac{3}{2f\tilde{\nu}^2} \quad (2)$$

where $\tilde{\nu}$ is the transition energy in cm^{-1}.

The emission spectra of PP and FPP have been predicted by MRCI and CASPT2 methods at the optimized excited-state geometries. The effect of a strong polar acetonitrile (MeCN) solvent on the excited state has been estimated by CASSCF calculations in connection of the polarized continuum model (PCM).[45] In the CASSCF treatment of the solvent effect, the active space is restricted within eight electrons distributed into seven relevant orbitals to reduce computational consumption. The 6-31G(d) basis set[46] was used in all calculations.

Results and Discussion

1. The Low-Lying States of PP and FPP. The CASSCF-optimized geometries of PP and FPP in their low-lying states are displayed respectively in Figures 1 and 2. For comparison, corresponding bond lengths by the X-ray analysis of the crystalline PP[34] and by previous calculations[27] are incorporated into Figure 1. The energies of the excited states relative to the ground state (GS) determined by CASSCF, MRCI, and CASPT2 calculations are shown in Tables 1 and 2.

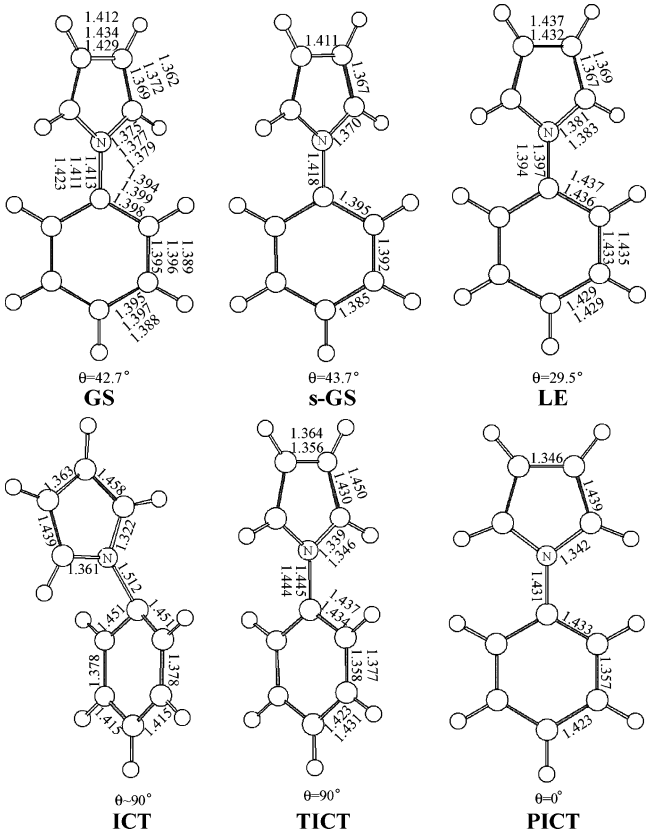

Figure 1. Geometries of the low-lying states in PP. The bond lengths given in an order of the present CASSCF value, previous theoretical value from ref 27, and experimental value from ref 34 are from inner to outer.

1.1. The Ground States. For PP, the internal rotation of the benzene and pyrrole rings around the molecular axis is dominated by *o*-hydrogen repulsion and π-electron conjugation of two rings in the gas phase. The *o*-hydrogen repulsion prefers a twisted structure, while the π-electron conjugation leads to a planar structure. The balance between both interactions gives rise to the ground-state structure with a dihedral angle of 38.7°, and the planar and perpendicular conformations are slightly higher than the lowest-energy structure by 457 and 748 cm^{-1}, respectively.[25] Such small barriers show that the PP molecule is quite flexible for the torsional motion as observed experimentally.[25]

Present CASSCF calculations predict that the ground state of PP has a twisted form with a twist angle of 42.7° between the benzene and pyrrole rings, which is in good agreement with the experimental values of ~38.7−42°.[23,25,47] As Figure 1 displays, the phenyl moiety retains a structure almost the same with benzene; the pyrrole moiety has a slightly more compact structure with shortened C7−C8 and C9−C10 bonds (refer to Chart 1) compared to the pyrrole molecule. Mulliken charge populations indicate that there are charge transfers of 0.33 *e* from C1 in the phenyl ring to the strongly electronegative N atom in the ground state of PP. The predicted dipole moment is −1.57 D in the gas phase, which agrees well with the experimental value of −1.39 D.[23]

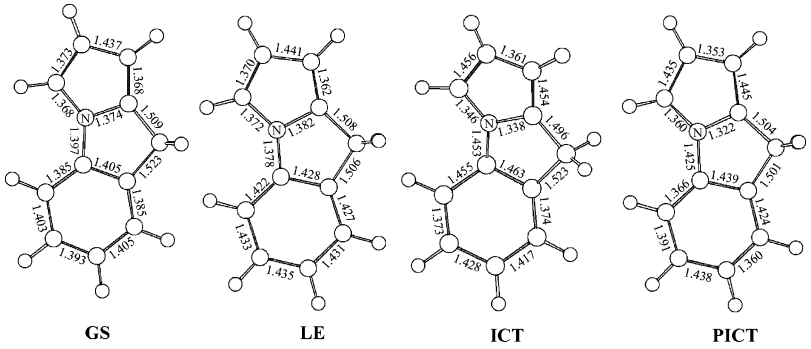

Figure 2. CASSCF-optimized geometries of the low-lying states in FPP.

TABLE 1: Relative Energies (ΔE, in eV), Dipole Moments (μ, in Debye), and Emission Energies (in eV) of the Low-Lying Singlet States in PP by Theory and Experiment

		ΔE			emission			μ	
state		CAS	MRCI	CASPT2	MRCI	CASPT2	exptl	present	exptl
GS	in gas	0	0	0				−1.57	−1.39[a]
	in MeCN							−2.08	
TGS	in gas	0.05	0.04	0.05				−1.99	
PGS	in gas	0.09	0.12	0.10				−1.16	
LE	in gas	4.72	4.81	4.52 (4.40[b])	4.53	4.35	4.10[c]	−1.01	−3.0; 1.6 ± 0.1[e]
	in MeCN			4.51		4.34	4.05[d]	−1.73	
PLE	in gas	4.75	4.87	4.55	4.51	4.28		−0.79	
	in MeCN			4.54		4.27			
TLE	in gas	4.84	4.97	4.78	4.67	4.55		−1.88	
ICT	in gas	5.69	5.31	4.94	3.37	3.52	3.65[f]	9.20	11.8 ± 1.0[e]
	in MeCN			4.63		3.22	3.48[g]	10.17	
	in MeCN						3.37[h]		
TICT	in gas	5.93	5.70	5.24	5.14	4.73		10.80	
	in MeCN			4.80		4.30		12.35	
PICT	in gas	5.95	5.83	5.29	5.11	4.65		9.00	
	in MeCN			4.89		4.24		11.33	

[a] Reference 23. [b] Reference 25. [c] Reference 34: LE fluorescence in the gas phase. [d] Reference 30: LE fluorescence in MeCN. [e] Reference 30. [f] Reference 24: CT fluorescence in MeCN. [g] Reference 34: CT fluorescence in MeCN. [h] Reference 35: CT fluorescence in MeCN at −45 °C.

TABLE 2: Relative Energies (ΔE, in eV), Dipole Moments (μ, in Debye), and Emission Energies (in eV) of the Low-Lying Singlet States in FPP by Theory and Experiment

		ΔE			emission			μ	
state		CAS	MRCI	CASPT2	MRCI	CASPT2	exptl	present	exptl[c]
GS	in gas	0	0	0		0	0	−1.22	−1.7
	in MeCN							−1.41	
LE	in gas	4.65	4.71	4.36	4.48	4.24		−0.41	∼−1
	in MeCN			4.36		4.24		−1.34	
	in MeCN						3.94[a]		
ICT	in gas	5.58	5.35	4.80	3.65	3.52		6.72	11 ± 0.4
	in MeCN			4.52		3.26		8.85	
	in MeCN						3.26[b]		
PICT	in gas	6.03	5.77	5.03	5.06	4.54		8.74	
	in MeCN			4.66		4.18		10.95	

[a] Reference 35: LE fluorescence in MeCN at 25 °C. [b] Reference 35: CT fluorescence in MeCN at 25 °C. [c] Reference 35: the dipole moment μ(ICT) has a direction opposite to that in the GS state.

The coplanar and perpendicular conformations of PP in the ground state (denoted as PGS and TGS, respectively) have quite similar bond lengths with the lowest-energy structure except a slightly longer N-phenyl bond in the perpendicular form due to loss of the weak π-electron conjugation. Actually, both benzene and pyrrole moieties are basically localized aromatic rings and their structures are less changed with the internal rotation. Predicted barriers for rotation of the lowest-energy PP to planar and perpendicular conformations are 0.10 and 0.05 eV, respectively, at the CASPT2 level of theory, and the internal rotation in the ground state around the molecular axis is thus very facile in the gas phase as observed experimentally.[25] This flexibility of the torsional motion of PP may make experimental observations unidentifiable such as ^{13}C NMR chemical shifts, and a near-planar conformation was assumed for PP in previous experiments.[24,48,49]

CHART 1

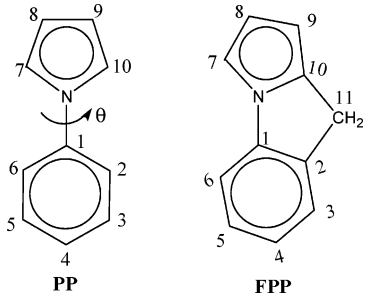

Since PP is a flexible molecule, the environment may play a significant role in determining its structure. For example, the crystalline PP has a near-planar conformation with a small twist angle of 5.7° by the X-ray analysis,[34] due to the crystal stacking effect. The most bonds in the crystal structure are slightly shorter than present and previous theoretical values, while the C1−N, N−C7, and N−C10 bonds are markedly longer. The long *N*-phenyl bond decreases *o*-hydrogen repulsion and stabilizes the near-planar crystal structure.

In consideration of the solvent effect, the ground-state PP in acetonitrile was optimized by CASSCF in connection of the PCM model. Calculations reveal that the solvent effect on the equilibrium geometry is almost negligible with respect to the gas phase. The ground-state geometry in acetonitrile has a similar skeleton with both the crystalline PP and the gas-phase PP, while the twist angle of two rings is 43.7°, larger than 42.7° in the gas phase. The polar solvent enhances the charge transfer from the phenyl to the pyrrole ring, resulting in a slightly larger dipole moment of −2.15 D than −1.57 D in the gas phase.

For FPP, the presence of a methylene linking pyrrole and phenyl rings results in a planar-rigidized structure, where phenyl and pyrrole rings of FPP slightly tilt toward the side of methylene as displayed in Figure 2. The optimized C1−N bond length is 1.397 Å, shorter than that of PP (1.413 Å) and similar to that of DMABN (1.396 Å).[19] The anticipated superconjugation interactions among the methylene and two aromatic rings will enhance the π-electron conjugation. The ground state of FPP has thus a perfect planar conformation. Unlike PP, the phenyl moiety of FPP in the GS has a long and short bond alternation as shown in Figure 2. The C2 and C3 atoms (refer to Chart 1) have little negative charge due to the electron donation of methylene. A small dipole moment of −1.22D is found for FPP, which is in the same direction as that of PP in the GS.

1.2. The Locally Excited States. The lower-energy LE state of PP located by the CASSCF optimization without symmetry restriction was found to be a twisted conformation. Compared with the ground state, the LE state has a relatively smaller twist angle (29.5°), shorter *N*-phenyl bond (1.397 Å), and an expanded phenyl ring with larger bond distance due to the local $\pi-\pi^*$ excitation within the phenyl moiety. The CASSCF-optimized geometries of PP in the LE state are consistent with previous theoretical[27] and experimental[25] studies. The geometrical features indicate that there is a relatively larger π-electron conjugation between the rings in the LE state compared with the ground state. Since the electronic excitation to the LE state is locally within the phenyl ring, no notable charge transfer between two rings occurs. Like the ground state, the LE state has a small dipole moment of −1.01 D in the gas phase or −1.73 D in the MeCN solution. The LE state is 4.52 eV above the ground state by CASPT2, which is comparable with the experimental value of 4.40 eV.[25]

The planar structure of the LE state (denoted as PLE) for PP was optimized by CASSCF within C_{2v} symmetry. The PLE conformation has quite similar skeleton structure with the LE state, and PLE and LE are almost isoenergetic as shown in Table 1. For the twisted structure of the LE state (TLE), the structural change with respect to the GS state basically focuses on the relaxation of the phenyl ring compared with the situation of the PLE. This can be ascribed to the complete decoupling between two rings in the perpendicular configuration. As Table 1 shows, the calculated energy barrier height to TLE from LE is higher than that to PLE, indicating that the rotation to perpendicular structure in the LE state is less facile, which agrees well with the spectroscopic investigation of the S_1-state torsional potential.[25]

CHART 2

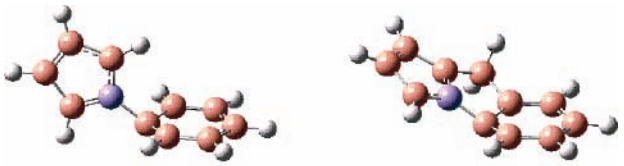

The lower-energy LE state of FPP has a planar structure with a shorter C1−N bond in comparison with the ground state. Like the situation of PP, the LE state of FPP is primarily contributed by the local $\pi-\pi^*$ excitation within the benzene moiety. Therefore, the LE state has also an expanded phenyl ring and a small dipole moment compared to the ground state as displayed in Figure 2 and Table 2. The LE state of FPP is calculated to be 4.36 eV above the ground state at the CASPT2 level. As Tables 1 and 2 show, both LE states of PP and FPP have quite similar relative energetics and dipole moments. It is noted that the LE states in Tables 1 and 2 are less changed in the polar MeCN solution with respect to the gas phase due to small dipole moments in both GS and LE states.

1.3. The ICT States. A lower-energy ICT state of PP with a twisted structure ($\theta \approx 90°$) has been located in the CASSCF optimization without symmetry constraint. The ICT state has a pyramidal C1 atom in the phenyl ring and a quinonoid phenyl ring (Chart 2). The C1 atom with a pyramidalization angle of ∼46° is out of the phenyl plane by ∼11°, while the nitrogen in the pyrrole ring is off the phenyl plane by ∼20° in an opposite direction. In the ICT state, the *N*-phenyl bond length is elongated by ∼0.10 Å with respect to the ground state. Such geometrical features in the ICT state of PP are quite similar to those in the ICT state of DMABN reported by Gómez et al.[20] Different from the LE state, the pyrrole ring exhibits notable changes both in geometry and in charge populations compared with the ground state. Frequency analysis shows that the lower-energy ICT structure is a stable minimum on the PES. Predicted dipole moments of the ICT state are 9.20 D in the gas phase and 10.17 D in the MeCN solution, which are in reasonable agreement with experimental value of 11.8 ± 1.0 D.[30]

The ICT state of PP has been investigated in previous theoretical calculations[14,26,27] within symmetry restriction or through the PES scanning along the torsion coordinate. The proposed ICT state is a twisted structure ($\theta = 90°$) without the C1 pyramidalization.[14,27] For comparison, we have also optimized the twisted ICT structure within C_{2v} symmetry (denoted as TICT) by CASSCF. Calculations indicate that the skeleton structure of TICT is basically the same as the lower-energy ICT state except a relatively shorter *N*-phenyl bond and longer C4−C3/C4−C5 bonds. The TICT conformation has a larger dipole moment of 10.80 D in the gas phase or 12.35 D in the MeCN solution, which also matches the experimental value. The TICT structure is 0.30 eV (0.17 eV in MeCN) higher in energy than the lower-energy ICT state at the CASPT2 level.

A planar charge-transfer conformation (denoted as PICT) also has been optimized by CASSCF. PICT has almost the same skeleton structure with TICT, where the *N*-phenyl bond length is 1.431 Å. The PICT conformation in C_{2v} symmetry is higher in energy than the lower-energy ICT state by 0.35 eV (0.26 eV in MeCN) at the CASPT2 level. Predicted dipole moments of the PICT structure in the gas phase and in the MeCN solution are 9.00 and 11.33 D, respectively.

TABLE 3: Calculated Vertical Transition Energies (ΔE, in eV), Oscillator Strengths (f), and Dipole Moments (μ, in Debye) of the Low-Lying Excited States in PP

state	character	μ	CASPT2 ΔE	f	TD ΔE	f	MRCI ΔE	CCSD ΔE	CAS ΔE	exptl ΔE
S_1	37 → 40 36 → 39	−1.04	4.69	0.0018	4.94	0.0086	4.94	5.12	4.82	
S_2	37 → 39	4.02	5.34	0.3429	5.13	0.3076	5.99	5.88	6.10	5.03[a], 4.86[b,c]
S_3	38 → 39	8.77	5.68	0.0103	4.64	0.0043	6.01	6.27	6.12	
S_4	38 → 40	11.27	6.00	0.0000	4.70	0.0000	6.37	6.75	6.50	

[a] Reference 24: in vapor. [b] Reference 24: in *n*-heptane. [c] Reference 25: in the gas phase (21 °C).

TABLE 4: Calculated Vertical Transition Energies (ΔE, in eV), Oscillator Strengths (f), and Dipole Moments (μ, in Debye) of Low-Lying Excited States in FPP

state	character	μ	CASPT2 ΔE	f	TD ΔE	f	MRCI ΔE	CCSD ΔE	CAS ΔE	exptl[a] ΔE
S_1	41 → 43, 39 → 42	−0.36	4.49	0.0124	4.72	0.0005	4.79	4.94	4.69	4.22
S_2	41 → 42	3.32	5.03	0.2730	5.02	0.3143	5.70	5.54	5.87	4.71
S_3	40 → 42	6.98	5.47	0.0205	4.79	0.0318	5.95	6.07	6.04	
S_4	40 → 43	9.01	5.55	0.1567	4.62	0.0001	6.17	6.35	6.32	

[a] Reference 35: in *n*-hexane.

The lower-energy ICT state of FPP is depicted in Figure 2. Because of the presence of methylene, the full rotation of two aromatic rings around the *N*-phenyl bond is impossible in the ICT state. The large charge transfer from the pyrrole ring to the phenyl moiety results in pyramidalization of the C1 atom in the phenyl ring (Chart 2). The C1 atom is out of the phenyl plane by ∼15° and the plane of the pyrrole ring and metheylene is off the phenyl ring by ∼34°. The deformation of the phenyl skeleton in the ICT state of FPP is much more remarkable compared with PP. In the ICT state of FPP, the *N*-phenyl bond length is enlarged by ∼0.06 Å with respect to the ground state. Similar to the ICT state of PP, the ICT state of FPP has a quinoidal phenyl ring and the bond-length alternation pyrrole ring. The calculated dipole moments in the gas phase and in the polar MeCN solution are 6.72 and 8.85 D, respectively, smaller than the experimental value.

Similarly, a PICT conformation of FPP is found to be 0.23 eV (0.14 eV in MeCN) higher in energy than the ICT state. The PICT structure of FPP has a dipole moment of 8.74 D in the gas phase or 10.95 D in the polar MeCN solution. In the PICT of FPP, the pyrrole moiety is similar to that of the ICT state, while the phenyl ring exhibits a distorted quinoidal structure, differing from that of the lower-energy ICT state. The *N*-phenyl bond length in PICT is intermediate between that of the ground state and that of the ICT state. Similar geometric features have been noticed in PICT of PP as mentioned above.

Present calculations show that various conformations of the electronic states with large dipole moments in both PP (ICT, TICT, and PICT) and FPP (ICT and PICT) have energy differences less than 6 kcal mol^{-1} with each other in MeCN, and they have similar bond-length distributions and charge separations. The lower-energy ICT states in both PP and FPP have significantly pyramidal deformation of the C1 atom connecting the pyrrole ring, in tune with the charge separation between rings. Small energy differences among ICT, TICT, and PICT imply that the internal rotation and the C1 atomic deformation in PP on the potential energy surface of the charge transfer state are facile. This can be attributed to the character of a single *N*-phenyl bond in the charge-transfer state.

2. Vertical Transition Energies and Absorption Spectra of PP and FPP. Properties of the low-lying states in both species have been calculated at the CASSCF-optimized geometries of their ground states. Predicted vertical excitation energies by different theoretical methods, corresponding oscillator strengths and dipole moments, as well as the character of the electronic excitation, are presented in Tables 3 and 4. For comparison,

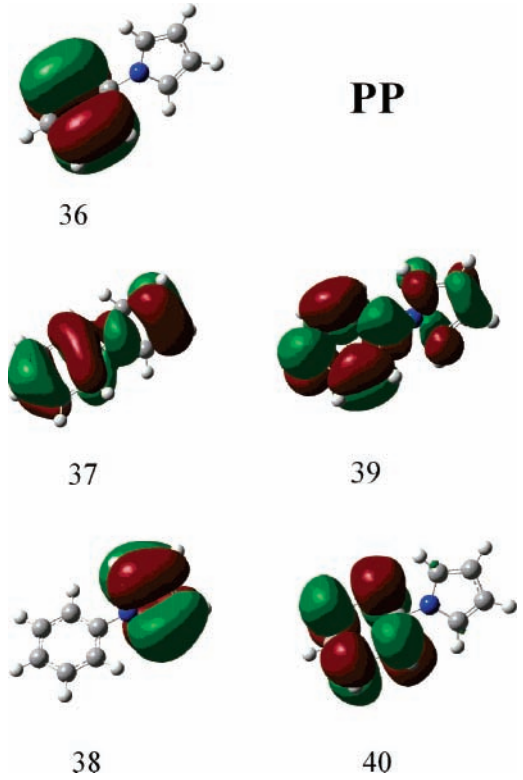

Figure 3. Relevant molecular orbitals involved in vertical electronic excitations to the low-lying states from the ground state in PP.

available experimental values are incorporated into Tables 3 and 4. The relevant molecular orbitals involved in these electronic excitations are depicted in Figures 3 and 4.

Inspection of results in Tables 3 and 4 reveals that the CASPT2 treatment has an accuracy of no more than 0.3 eV in comparison with available experimental values. The TD-B3LYP approach is also applicable for certain strong absorptions. However, the TD-B3LYP treatment badly underestimates transition energies for the charge-transfer excited states with large dipole moments in comparison with the CASPT2 and MRCI calculations. In contrast, due to loss of the dynamical electron correlation, the CASSCF method strikingly overestimates vertical transition energies. Present MRCI calculations have no notable improvement for the description of the vertical low-lying states with respect to the CASSCF treatment owing to involvement of less-active molecular orbitals in calculation. As Tables 3 and 4 display, the CCSD-EOM calculations exhibit

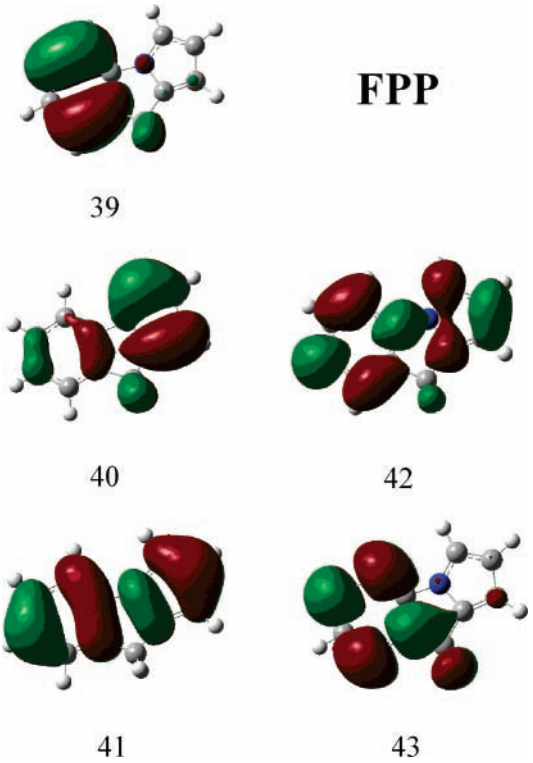

Figure 4. Relevant molecular orbitals involved in vertical electronic excitations to the low-lying states from the ground state in FPP.

the same energy order of the low-lying excited states with the MRCI and CASPT2 treatments, while the calculated transition energies are generally larger than those obtained by other sophisticated multireference methodologies. A comparison of these predicted vertical transition energies reveals that the reliable description of the low-lying states in PP and FPP requires the multireference methodology incorporating dynamical electron correlation.

For PP, the electronic excitation to the first singlet excited state (S_1) occurs at 4.69 eV ($f = 0.0018$) at the CASPT2 level. S_1 is a LE state principally contributed by the electronic excitations from the 37th orbital (highest-occupied molecular orbital (HOMO)-1) to the 40th orbital (lowest-unoccupied molecular orbital (LUMO)+1) and from the 36th orbital (HOMO-2) to the 39th orbital (LUMO) (refer to Figure 3). The strongest absorption in PP appears at 5.34 eV ($f = 0.3429$) by CASPT2 or 5.13 eV by TD-B3LYP, which arises from the electronic excitation to the second singlet state (S_2). The electron promotion from the 37th orbital to the 39th orbital is responsible for S_2, and S_2 has a dipole moment of 4.02 D. CASPT2 calculations predict two higher-energy singlet states S_3 and S_4 lie at 5.68 and 6.00 eV above the ground state, respectively. As Table 3 and Figure 3 display, both S_3 and S_4 have large dipole moments of 8.77 and 11.27 D, respectively, which arise from corresponding charge-transfer excitations from the 38th−39th orbital and from the 38th−40th orbital. The 38th orbital (HOMO) is completely localized at the pyrrole ring, while the 39th (LUMO) and 40th MOs are mainly distributed at the phenyl ring as shown in Figure 3. Because of the negligible oscillator strength for the electronic excitation to S_4, it is thus not accessible by the direct CT transition.

Since PP is quite flexible for the internal rotation in the ground state, the vertical electronic transitions at the planar and twisted conformations have been examined to explore the effect of torsional motion on the absorption spectra of PP. The vertical transition energies of PP in the PGS and TGS configurations are collected in Table 5.

TABLE 5: Vertical Transition Energies (ΔE, in eV), Oscillator Strengths (f), and Dipole Moments (μ, in Debye) of Low-Lying Excited States by CASPT2 at the Geometries of PGS and TGS in PP

PGS state	ΔE	f	μ	TGS state	ΔE	f	μ
1^1B_2	4.74	0.0042	−0.71	1^1B_2	4.92	0.0001	−3.15
2^1A_1	5.14	0.4220	3.21	2^1B_2	5.38	0.0000	11.60
2^1B_2	5.74	0.0099	6.60	2^1A_1	6.00	0.0130	−5.03
3^1A_1	6.03	0.1386	10.00	1^1A_2	6.08	0	11.26

As shown in Table 5, the vertical excitations below ∼6 eV at the TGS conformation have very small oscillator strengths, which are unlikely involved in experimental absorption spectra of PP. The vertical transitions from the PGS geometry are very similar to those of the GS structure, where strong absorptions occur at 5.14 ($f = 0.422$) and 6.03 eV ($f = 0.1386$), respectively. The strong electronic transitions at 5.34 eV (GS) or at 5.14 eV (PGS) can be responsible for the experimental band at 5.03 eV.[24] Presumably, with increase of the excitation energy, the direct CT transition at ∼6 eV is likely in the gas phase. These results show that the internal rotation in PP will significantly modify accessibility of the low-lying states while the relative energetics is less changed.

For FPP, the first singlet excited state (S_1) lies at 4.49 eV ($f = 0.0124$) above the ground state by CASPT2. The electronic transition to S_1 corresponds to the weak absorption at 4.22 eV in experiment.[35] Predicted strongest GS → S_2 transition occurs at 5.03 eV, which reasonably agrees with the experimental band at 4.71 eV.[35] S_3 and S_4 with the charge-transfer character appear at 5.47 eV ($f = 0.0205$) and 5.55 eV ($f = 0.1567$), respectively. Both states are slightly lower in energy than those of PP owing to the presence of methylene, whereas the photophysical activity of S_4 in PP and FPP is totally different. S_4 in PP has negligible oscillator strength, while in the S_4 state of FPP the oscillator strength is 0.1567, more like the case of PGS in PP. This can be ascribed to a commonly planar configuration in the GS of FPP and the PGS of PP. It can be seen from Tables 3 and 4 that the photophysical properties of S_1 and S_2 in both PP and FPP are quite similar.

3. Emission Spectra and Dual Fluorescence Mechanisms in PP and FPP. On the basis of the optimized structures of the LE and ICT states, their fluorescence emissions have been explored. The solvent effect in acetonitrile has been estimated within the PCM model by CASSCF. Calculated results are incorporated into Tables 1 and 2.

In PP, the LE state decays to the ground state with a fluorescence emission of 4.35 eV in the gas phase by CASPT2. The predicted fluorescence emission is comparable with the experimental band at 4.10 eV.[34] Since PLE has similar photophysical properties with the lower-energy LE state as shown in Table 1, it also contributes to the normal fluorescence emission. Because of a small dipole moment for LE, the calculated emission energy in the polar acetonitrile solution is similar to that in the gas phase. In FPP, the predicted fluorescence emission of the LE state occurs at 4.24 eV, slightly larger than the experimental observation of 3.94 eV.[35]

As shown in Tables 1, CASPT2 calculations predict the fluorescence emission of the lower-energy ICT state of PP at 3.52 eV in the gas phase or at 3.22 eV in MeCN, which is in reasonable agreement with the experiment bands in a region of ∼3.37−3.65 eV.[24,34,35] Similarly, the predicted fluorescence emission of the lower-energy ICT state of FPP occurs at 3.52 eV in the gas phase or at 3.26 eV in MeCN, which matches the

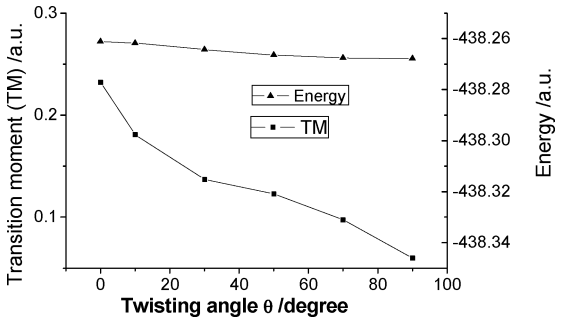

Figure 5. The ICT-GS state−state transition dipole moments and energies of the lower-energy ICT state are plotted as a function of torsional angle θ in PP.

experimental value of 3.26 eV very well.[35] These results support that the lower-energy ICT states in PP and FPP are responsible for the red-shifted fluorescence bands observed experimentally.[34,35]

As Tables 1 and 2 display, the calculated emission energies of PICT and TICT for PP and FPP are much higher than those of the lower-energy ICT states as well as the red-shifted experimental bands. Therefore, these CT configurations cannot be served as the carriers of the red-shifted fluorescence. Provided that both PICT and TICT conformations are accessible, their emissions are unidentifiable due to emissions of PICT and TICT close to the normal LE fluorescence band in MeCN.

Dependence of the ICT emission on the torsional angle for PP has been investigated to elucidate the mechanism of dual fluorescence. Generally, the dipole radiative transition is determined by the transition moment. Figure 5 displays the vertical state−state transition dipole moment from the lower-energy ICT state to the ground state as a function of torsional angle around the *N*-phenyl bond in PP. As Figure 5 shows, with the decrease of twisting angle θ from 90 to 0°, the ICT-GS transition moment strikingly increases, while corresponding energy gains from a twisted conformation to planar form of the lower-energy ICT state are less than 3.2 kcal mol^{-1} at the CASPT2 level. Such small fluctuation in energy and outstanding change in transition moment reveal that the internal rotation in the lower-energy ICT state significantly modify the activity of the ICT state instead of the emissive energy of the ICT state. Therefore, a planar conformation of the ICT state with the C1 pyramidalization plays an important role in the red-shifted fluorescence emission experimentally.

For both TICT and PICT states without the C1 deformation, transition moment calculations indicate that the PICT state has largest emissive activity and the transition dipole moment gradually decreases as the twisting angle increases.

As Tables 3 and 4 show, CASPT2 calculations systematically overestimate the vertical transition energies by ∼0.3 eV. In addition, the S_2 state can be stabilized by ∼0.2 eV in the acetonitrile solvent with respect to the ground state. In consideration of the computational deviation and the solvent effect, the S_2 states of PP and FPP with large oscillator strengths are easily accessible under the experimental excitation at ∼265 nm for PP or at 270 nm for FPP. By combination of present calculations with analyses of photophysical properties, we can rationalize plausible dual fluorescence mechanism of PP and FPP as follows

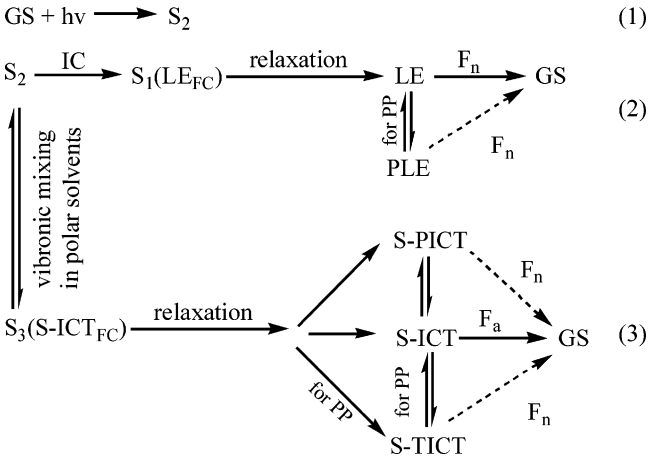

As Figures 6 and 7 display, the ground states of FPP and PP are vertically excited to the S_2 states first. The S_2 state has a very short lifetime of $\sim 10^{-9}$ s, and it will decay to S_1, a Franck−Condon state of LE (LE_{FC}), through fast internal conversion (IC) because of large state−state transition dipole moments ($TM(S_2-S_1) = 0.18$ au for PP and $TM(S_2-S_1) = 0.32$ au for FPP). Followed by the geometrical relaxation of S_1, the lower-energy LE is formed. The LE state emits the normal fluorescence back to the ground state. As discussed above, LE and its planar counterpart PLE in PP have quite similar photoexcitation properties, and both conformations are likely responsible for the normal fluorescence emission, although the PLE form is less stable than the LE state. In the gas phase, the ICT states with large dipole moments are fairly higher in energy than the LE states, so that they cannot be populated under the low-energy excitation light. In this case, only one normal fluorescence band appears in the gas-phase fluorescence spectra as observed experimentally.[34,35]

In the polar acetonitrile solvent, the vertical excitation energy of the solvated S_3 state with charge-transfer character ($S\text{-}ICT_{FC}$)

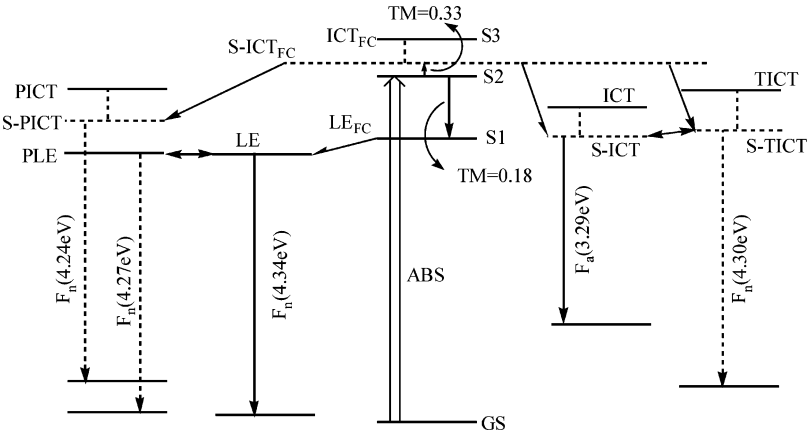

Figure 6. The dual fluorescence mechanism of PP (TM = transition dipole moment).

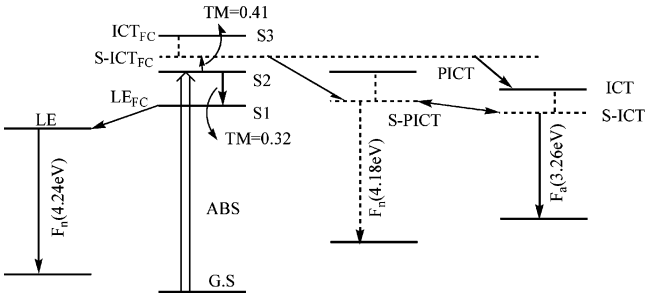

Figure 7. The dual fluorescence mechanism of FPP (TM = transition dipole moment).

is lowered remarkably. Consequently, the small energy difference and large state−state transition dipole moment (TM = 0.33 au for PP, and TM = 0.41 au for FPP) between S_2 and S-ICT$_{FC}$ make the S-ICT$_{FC}$ state is accessible through the vibronic interactions in acetonitrile. Upon formation of the S-ICT$_{FC}$ state, it will decay to the more stable solvated ICT states (S−ICT) through the geometrical relaxation. The lower-energy S-ICT states of FPP and PP are responsible for the red-shifted fluorescences in the polar MeCN solution.

For PP, S-PICT, S-TICT, and the lower-energy S-ICT forms with C1 pyramidalization and different torsional angles are likely to come into being from the S-ICT$_{FC}$ state due to the flat PES of the charge-transfer state in acetonitrile. Once S-PICT and S-TICT are populated, they both can directly emit fluorescence back to PGS and TGS, respectively. The calculated emission energies of the S-PICT and S-TICT conformations are comparable with the normal LE emission. Such fluorescence emissions will be thus buried in the normal band, even if the less stable S-PICT and S-TICT forms might be accessed.

For FPP, the possibility for the direct CT transition to the S-ICT$_{FC}$ state cannot be ruled out in the polar solvent, along with the S_2 population. Moreover, the PICT conformation has a planar structure similar to the ground state so that the solvated PICT form (S-PICT) is possible to be populated in the formation of S_2. Upon formation of S-PICT, the less stable S-PICT relaxes to the lower-energy S-ICT state through pyramidalization of the C1 atom in the phenyl ring. On the other hand, the S-PICT conformation emits fluorescence directly back to the ground state. Such emission will overlap with the normal LE band.

Concluding Remarks

PP and its planar-rigidized derivative FPP have been comparatively investigated by extensive calculations. The ground state of PP has a twisted structure both in the gas phase and in the polar acetonitrile solution. Because of the presence of methylene, FPP in the ground state has a planar structure. Calculations show that the vertical transition energies of PP and FPP are similar to each other. The strongest absorption corresponds to the electronic excitation to S_2. S_2 is a precursor to consecutively photophysical processes. In PP, the internal rotation is quite facile in the gas phase, which makes the planar and perpendicular configurations of PP accessible in the photoexcitation process. The higher-energy states S_3 and S_4 from the CT excitations have large dipole moments and they can be stabilized significantly in the polar solvent. Predicted vertical transition energies reasonably agree with available experimental values.

The lower-energy LE state of PP has a smaller twist angle between two rings with respect to the ground state. On the PES of LE, the barrier to the planar structure is much small than that to the perpendicular structure. Both LE and PLE conformations may contribute to the LE fluorescence, resulting in a stronger normal emission than the red-shifted band.

Various conformations of the ICT state in both PP and FPP have comparable stability within 6 kcal mol^{-1} in MeCN. They have similar bond-length distributions and charge separations. The twisting of molecule around the *N*-phenyl bond is thus not necessary for the ICT in PP. The quinoidization of phenyl ring in combination with the *N*-phenyl bond elongation generally characterizes the ICT. The pyramidal deformation of the C1 atom in the phenyl ring can tune with the charge separation and it generally characterizes the lower-energy ICT state geometrically for both PP and FPP. Present results show that only the ICT states with pyramidal deformation of the C1 atom connecting the pyrrole ring are responsible for the anomalous red-shifted fluorescence bands for both PP and FPP. Particularly, although the twisting form of the lower-energy ICT state of PP is slightly more stable than its planar counterpart, the planar conformation of the lower-energy ICT state will be basically responsible for the red-shifted fluorescence emission due to its significant photophysical activity.

The polar solvent plays a crucial role in the dual fluorescence mechanism of PP and FPP. The polar solvent stabilizes the low-lying states with the CT character, which makes the solvated ICT$_{FC}$ states accessible through vibronic interactions coupling S_2 to relevant CT states. The decay of the solvated ICT$_{FC}$ state leads to the lower-energy solvated ICT state.

Since the lower-energy ICT state is only higher in energy than the lower-energy LE state by ∼0.12−0.16 eV in MeCN at the CASTP2 level, the LE ↔ICT charge transfer reaction may take place if the LE state lies at a thermally vibrational state.

Acknowledgment. We thank the National Science Foundation (Project Nos. 20473062, 20233020, 20021002, and 20173042), the Ministry of Science and Technology (Project Nos. 2004CB719902 and 001CB1089), and the Ministry of Education for generously supporting this work.

References and Notes

(1) Lippert, E.; Lüder, W.; Moll, F.; Nägele, W.; Boos, H.; Prigge, H.; Seybold-Blankenstein, I. *Angew. Chem.* **1961**, *73*, 695.

(2) Lippert, E.; Lüder, W.; Boos, H. In *Advances in Molecular Spectroscopy, European Conference on Molecular Spectroscopy*; Mangini, A., Ed.; Pergamon Press: Oxford, 1962; pp 443−457.

(3) Grabowski, Z. R.; Rotkiewicz, K.; Rettig, W. *Chem. Rev.* **2003**, *103*, 3899 and its references.

(4) Rotkiewicz, K.; Grellmann, K. H.; Grabowski, Z. R. *Chem. Phys. Lett.* **1973**, *19*, 315; **1973**, *21*, 212.

(5) Grabowski, Z. R.; Rotkiewicz, K.; Siemiarczuk, A.; Cowley, D. J.; Baumann, W. *Nouv. J. Chim.* **1979**, *3*, 443.

(6) Zachariasse, K. A.; Von der Haar, Th.; Hebecker, A.; Leinhos, U.; Kühnle, W. *Pure. Appl. Chem.* **1993**, *65*, 1745.

(7) Von der Haar, Th.; Hebecker, A.; Il'ichev, Yu. V.; Jiang, Y.-B.; Kühnle, W.; Zachariasse, K. A. *Recl. Trav. Chim. Rays-Bas.* **1995**, *114*, 430.

(8) Zachariasse, K. A.; Grobys, M.; Von der Haar, Th.; Hebecker, A.; Il'ichev, Yu. V.; Jiang, Y.-B.; Morawski, O.; Kühnle, W. *J. Photochem. Photobiol., A* **1996**, *102*, 59.

(9) Zachariasse, K. A.; Grobys, M.; Von der Haar, Th.; Hebecker, A.; Il'ichev, Yu. V.; Morawski, O.; Rückert, I.; Kühnle, W. *J. Photochem. Photobiol., A* **1997**, *105*, 373.

(10) Schuddeboom, W.; Jonker, S. A.; Warman, J. M.; Leinhos, U.; Kühnle, W.; Zachariasse, K. A. *J. Phys. Chem.* **1992**, *96*, 10809.

(11) Gorse, A. D.; Pesquer, M. *J. Phys. Chem.* **1995**, *99*, 4039.

(12) Sobolewski, A. L.; Domcke, W. *Chem. Phys. Lett.* **1996**, *250*, 428.

(13) Sobolewski, A. L.; Domcke, W. *Chem. Phys. Lett.* **1996**, *259*, 119.

(14) Zilberg, S.; Haas, Y. *J. Phys. Chem. A* **2002**, *106*, 1.

(15) Lippert, E.; Rettig, W.; Bonacic-Koutecký, V.; Heisel, F.; Miehé, J. A. *Adv. Chem. Phys.* **1987**, *68*, 1.

(16) Changenet, P.; Plaza, P.; Martin, M. M.; Meyer, Y. H. *J. Phys. Chem. A* **1997**, *101*, 8186 and references therein.

(17) Fuss, W.; Pushpa, K. K.; Rettig, W.; Schmid, W. E.; Trushin, S. A. *Photochem. Photobiol. Sci.* **2002**, *1*, 255.
(18) Rappoport, D.; Furche, F. *J. Am. Chem. Soc.* **2004**, *126*, 1277.
(19) Xu, X. F.; Cao, Z. X.; Zhang, Q. E. *J. Chem. Phys.* **2005**, *122*, 194305.
(20) Gómez, I.; Reguero, M.; Boggio-Pasqua, M.; Robb, M. A. *J. Am. Chem. Soc.* **2005**, *127*, 7119.
(21) Rettig, W.; Marschner, F. *New. J. Chem.* **1983**, *7*, 425.
(22) Rettig, W.; Marschner, F. *New J. Chem.* **1990**, *14*, 819.
(23) Lumbroso, H.; Bertin, D. M.; Marschner, F. *J. Mol. Struct.* **1988**, *178*, 187.
(24) Sarkar, A.; Chakravorti, S. *Chem. Phys. Lett.* **1995**, *235*, 195.
(25) Okuyama, K.; Numata, Y.; Odawara, S.; Suzuka, I. *J. Chem. Phys.* **1998**, *109*, 7185.
(26) Parusel, A. B. J. *Phys. Chem. Chem. Phys.* **2000**, *2*, 5545.
(27) Proppe, B.; Merchán, M.; Serrano-Andrés, L. *J. Phys. Chem. A* **2000**, *104*, 1608.
(28) Belau, L.; Haas, Y.; Rettig, W. *Chem. Phys. Lett.* **2002**, *364*, 157.
(29) Manz, J.; Proppe, B.; Schmidt, B. *Phys. Chem. Chem. Phys.* **2002**, *4*, 1876.
(30) Yoshihara, T.; Galievsky, V. A.; Druzhinin, S. I.; Saha, S.; Zachariasse, K. A. *Photochem. Photobiol. Sci.* **2003**, *2*, 342.
(31) Schweke, D.; Haas, Y. *J. Phys. Chem. A* **2003**, *107*, 9554.
(32) Belau, L.; Haas, Y.; Rettig, W. *J. Phys. Chem. A* **2004**, *108*, 3916.
(33) Schweke, D.; Baumgarten, H.; Haas, Y.; Rettig, W.; Dick, B. *J. Phys. Chem. A* **2005**, *109*, 576.
(34) Yoshihara, T.; Druzhinin, S. I.; Demeter, A.; Kocher, N.; Stalke, D.; Zachariasse, K. A. *J. Phys. Chem. A* **2005**, *109*, 1497.
(35) Yoshihara, T.; Druzhinin, S. I.; Zachariasse, K. A. *J. Am. Chem. Soc.* **2004**, *126*, 8535.
(36) (a) Werner, H.-J.; Knowles, P. J. *J. Chem. Phys.* **1985**, *82*, 5053. (b) Knowles, P. J.; Werner, H.-J. *Chem. Phys. Lett.* **1985**, *115*, 259. (c) Busch, T.; Degli Esposti, A.; Werner, H.-J. *J. Chem. Phys.* **1991**, *94*, 6708. (d) Roos, B. O. In *Ab Initio Methods in Quantum Chemistry II*; Lawley, K. P., Ed.; Wiley: New York, 1987; p 399.
(37) Werner, H.-J.; Knowles, P. J.; Amos, R. D.; Bernhardsson, A.; Berning, A.; Celani, P.; Cooper, D. L.; Deegan, M. J. O.; Dobbyn, A. J.; Eckert, F.; Hampel, C.; Hetzer, G.; Knowles, P. J.; Korona, T.; Lindh, R.; Lloyd, A. W.; McNicholas, S. J.; Manby, F. R.; Meyer, W.; Mura, M. E.; Nicklass, A.; Palmieri, P.; Pitzer, R.; Rauhut, G.; Schütz, M.; Schumann, U.; Stoll, H.; Stone, A. J.; Tarroni, R.; Thorsteinsson, T.; Werner, H.-J. *MOLPRO*, version 2002.1.
(38) Frisch, M. J.; Trucks, G. W.; Schlegel, H. B.; Scuseria, G. E.; Robb, M. A.; Cheeseman, J. R.; Zakrzewski, V. G.; Montgomery, J. A., Jr.; Stratmann, R. E.; Burant, J. C.; Dapprich, S.; Millam, J. M.; Daniels, A. D.; Kudin, K. N.; Strain, M. C.; Farkas, O.; Tomasi, J.; Barone, V.; Cossi, M.; Cammi, R.; Mennucci, B.; Pomelli, C.; Adamo, C.; Clifford, S.; Ochterski, J.; Petersson, G. A.; Ayala, P. Y.; Cui, Q.; Morokuma, K.; Malick, D. K.; Rabuck, A. D.; Raghavachari, K.; Foresman, J. B.; Cioslowski, J.; Ortiz, J. V.; Stefanov, B. B.; Liu, G.; Liashenko, A.; Piskorz, P.; Komaromi, I.; Gomperts, R.; Martin, R. L.; Fox, D. J.; Keith, T.; Al-Laham, M. A.; Peng, C. Y.; Nanavakkara, A.; Gonzalez, C.; Challacombe, M.; Gill, P. M. W.; Johnson, B.; Chen, W.; Wong, M. W.; Andres, J. L.; Gonzalez, C.; Head-Gordon, M.; Replogle, E. S.; Pople, J. A. *Gaussian 98*, revision A.9; Gaussian, Inc.; Pittsburgh, PA, 1998.
(39) Parusel, A. B. J.; Rettig, W.; Sudholt, W. *J. Phys. Chem. A.* **2002**, *106*, 804.
(40) (a) Werner, H.-J.; Knowles, P. J. *J. Chem. Phys.* **1988**, *89*, 5803. (b) Knowles, P. J.; Werner, H.-J. *Chem. Phys. Lett.* **1988**, *145*, 514. (c) Knowles, P. J.; Werner, H.-J. *Theor. Chim. Acta* **1992**, *84*, 95.
(41) (a) Werner, H.-J. *Mol. Phys.* **1996**, *89*, 645. (b) Celani, P.; Werner, H.-J. *J. Chem. Phys.* **2000**, *112*, 5546.
(42) Casida. M. E.; Jamorski. C.; Casida, K. C.; Salahub, D. R. *J. Chem. Phys.* **1998**, *108*, 4439.
(43) Hampel, C.; Peterson, K.; Werner, H.-J. *Chem. Phys. Lett.* **1992**, *190*, 1.
(44) Peyerimhoff, S. D. In *The Encyclopedia of Computational Chemistry*; Schleyer, P. v. R., Allinger, N. L., Clark, T., Gasteiger, J., Kollman, P. A., Schaefer, H. F., III, Schreiner, P. R., Eds.; Wiley: Chichester, 1998; Vol. 4, pp 2646−2664.
(45) Cossi, M.; Barone, V.; Robb, M. A. *J. Chem. Phys.* **1999**, *111*, 5295.
(46) (a) Herhe, W. J.; Ditchfield, R.; Pople, J. A. *J. Chem. Phys.* **1972**, *56*, 2257. (b) Harihan, P. C.; Pople, J. A. *Theor. Chim. Acta.* **1973**, *28*, 213.
(47) Schomaker, V.; Pauling, L. *J. Am. Chem. Soc.* **1939**, *61*, 1769.
(48) Fong, C. W. *Aust. J. Chem.* **1980**, *33*, 1763.
(49) Jones, R. A.; Spotswood, T. McL.; Cheuychit, P. *Tetrahedron* **1967**, *23*, 4469.